

Virtual Indicative Broadband over Power Lines Topologies for Respective Subclasses by Adjusting Channel Attenuation Statistical Distribution Parameters of Statistical Hybrid Models (Class Maps) – Part 3: The Case of Overhead Transmission Power Grids

Athanasios G. Lazaropoulos*

School of Electrical and Computer Engineering / National Technical University of Athens / 9 Iroon Polytechniou Street / Zografou, GR 15780

Received June 21, 2019; Accepted August 12, 2019; Published August 16, 2019

In [1], [2], the theoretical framework and the numerical results concerning the class mapping of overhead and underground medium voltage broadband over power lines (OV and UN MV BPL) topologies have been presented on the basis of the recently proposed initial statistical hybrid model (iSHM), modified statistical hybrid model (mSHM) and class map definition procedure. In this paper, all the recent findings regarding the statistical channel modeling and class mapping are first applied to transmission BPL networks; say, OV high voltage (HV) BPL topologies. The numerical results of OV HV BPL networks are compared against the respective ones of OV and UN distribution networks revealing significant similarities and differences. Finally, the impact of considering minimum or maximum capacity value instead of the average one during the definition procedure is investigated as well as the behavior of the total simulation time of class mapping.

Keywords: Smart Grid; Broadband over Power Lines (BPL) networks; Power Line Communications (PLC); Distribution Power Grids; Capacity; Statistics; Modeling

1. Introduction

As the BPL channel modeling is concerned for the distribution and transmission Broadband over Power Lines (BPL) networks, BPL channel models have typically followed either a bottom-up approach or a top-down approach or appropriate synergies of the aforementioned approaches until now [3]-[25]. Recently, statistical channel models have been proposed for BPL networks [26]-[33]. Among them, statistical hybrid models (SHMs) are based on the formality and validity of the deterministic hybrid model, which interconnects the bottom-up and top-down approach and has extensively been validated in transmission and distribution BPL networks [5]-[10], [13], [15], [16], [20], [34], while SHMs results are considered as the filtered deterministic hybrid model results through a set of proper channel attenuation statistical distributions (CASDs). Initial SHM (iSHM), which has been proposed in [28], [29], applies well-known CASDs of the communications research fields, such as Gaussian,

*Corresponding author: AGLazaropoulos@gmail.com

Lognormal, Wald, Weibull and Gumbel CASDs [35], while modified SHM (mSHM), which has been proposed in [30], exploits the Empirical CASD. As already been mentioned in [28]-[30], CASD parameters, which are CASD maximum likelihood estimators (MLEs) and CASD cumulative density functions (CDFs) for iSHM and mSHM, respectively, can characterize each real distribution BPL topology while virtual distribution BPL topologies can be defined by appropriately adjusting the aforementioned CASD parameters [1], [2]. The significance of the combined operation of SHMs with the definition procedure of the virtual indicative distribution BPL topologies, which has been presented in [28], [29], mitigates the underrepresentation of the distribution BPL topology classes during the BPL statistical channel modelling and the graphical representation of the distribution BPL topology classes and subclasses in terms of their average capacity through the proposed class maps. In this paper, all the recent findings concerning iSHM, mSHM, CASDs, CASD parameters, definition procedure and class maps are first applied to OV HV BPL topologies in this paper. The results for the transmission BPL networks are compared against the ones of distribution BPL networks. Interesting similarities and differences can be unveiled between the distribution and transmission BPL networks since the different BPL signal transmission characteristics can influence in different ways the behavior of CASDs and, thus, of iSHM and mSHM. Also, an interesting contribution to the definition procedure is the impact examination of applying maximum and minimum capacity value of the distribution BPL topology subclasses instead of the average one. Finally, the theoretical approach of the total simulation time of iSHM and mSHM class mapping is here graphically investigated in terms of the time complexity when different number of spacings, that is a critical factor of class mapping for the accuracy of the x- and y-axis, are applied during the iSHM and mSHM class mapping.

The rest of this paper is organized as follows: In Section II, the OV HV MTL configuration with the set of indicative OV HV BPL topologies of the main topology subclasses are presented. In Section III, the numerical results concerning the application of iSHM and mSHM are demonstrated as well as the respective CASD parameter analysis, definition procedure and class maps. Also, a comparative analysis is given between the distribution and transmission BPL topologies. Section IV concludes this paper.

2. OV HV MTL Configurations and Respective BPL Topologies

Similarly to [1], a small briefing concerning the adopted OV HV MTL configuration is given while the topological characteristics of the indicative OV HV BPL topologies of the main subclasses are reported.

2.1 OV HV MTL Configurations

In Fig. 1, the typical OV HV MTL configuration that is used in the present work is illustrated. The MTL configuration of this paper is a typical OV 400kV double-circuit configuration with phase lines of radius r_p^{OVHV} that hang at typical heights h_p^{OVHV} above ground *-i.e.*, conductors 1, 2, 3, 4, 5, and 6-. These six phase conductors are divided into three bundles. Each bundle is spaced by $\Delta_{p1}^{\text{OVHV}}$ while the phase conductors of each bundle

are connected by non-conducting spacers and are separated by Δ_{p2}^{OVHV} . Apart from the phase conductors, two parallel neutral conductors hang at heights h_n^{OVHV} —i.e, conductors 7 and 8—. Neutral conductors are of radius r_n^{OVHV} and are spaced each other by Δ_n^{OVHV} .

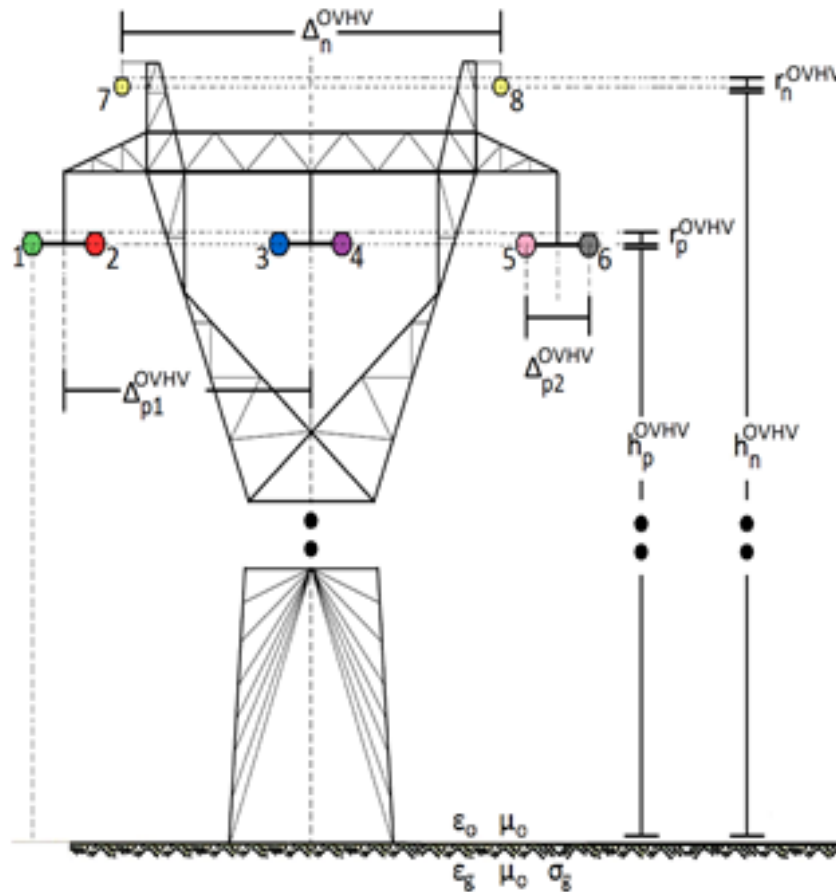


Fig. 1. Typical OV HV MTL configuration [9].

All phase and neutral conductors are Aluminium-conductor steel-reinforced (ACSR) [4], [9], [36]-[39]. The exact dimensions concerning the radii, spacings and heights are given in [9].

Similarly to distribution BPL networks, the ground is considered imperfect and as the reference conductor. A realistic scenario, which is adopted in this paper, holds that the conductivity of the ground is assumed $\sigma_g = 5 \text{ mS/m}$ while its relative permittivity $\epsilon_g = 13$ [4]-[6], [9], [13], [40]-[44].

2.2 OV HV BPL Topologies and Respective Topology Subclasses and Classes

Transmission BPL topologies adopt the network architecture of distribution BPL topologies. Actually, transmission BPL networks are divided into cascaded BPL topologies of typical lengths of 25km. Similarly to distribution BPL topologies, each transmission BPL topology is bounded by its transmitting and receiving end while

different number of branches $k, k = 1, \dots, N$, distribution cable lengths $L_k, k = 1, \dots, N+1$ and branch lengths $L_{bk}, k = 1, \dots, N$ are encountered between the transmitting and receiving end [5]-[10], [34].

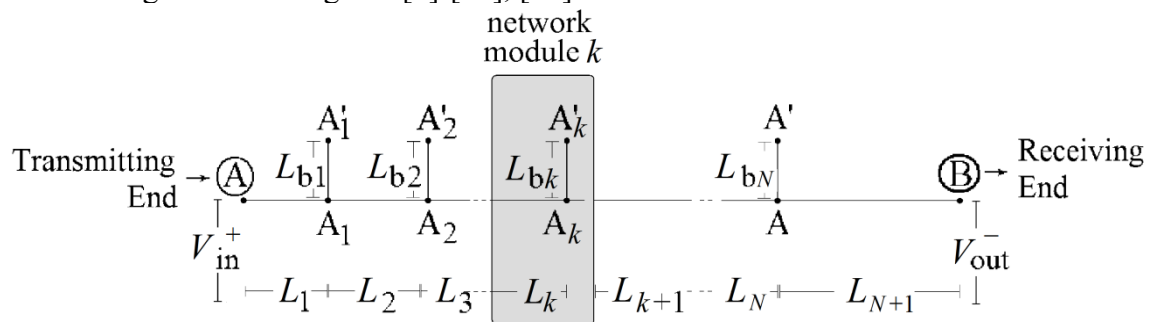


Fig. 2. Typical OV HV BPL topology with N branches [1].

As the BPL signal transmission across the transmission BPL topologies is concerned, the following five indicative OV HV BPL topologies of the main subclasses of the respective transmission BPL topology classes are examined, namely [4], [9], [45]: (i) A typical OV HV BPL urban topology (simply denoted as urban case A); (ii) An aggravated OV HV BPL urban topology (simply denoted as urban case B); (iii) A typical suburban OV HV BPL topology (simply denoted as suburban case); (iv) A typical OV HV BPL rural topology (simply denoted as rural case); and (v) The “LOS” transmission along the same end-to-end distance $L=L_1+\dots+L_{K+1}=25\text{km}$. This topology corresponds to Line of Sight transmission of wireless channels (simply denoted as “LOS” case). The topological characteristics of the aforementioned five indicative OV HV BPL topologies of the main subclasses are reported in Table 1.

Table 1. Indicative OV HV BPL Topologies of the Main Subclasses and Respective BPL Topology Classes

OV HV BPL Topology Class	BPL Topology Number (and BPL Topology Subclass Number) (I)	BPL Topology Name (and BPL Topology Subclass Name)	Number of Branches	Length of Distribution Lines	Length of Branching Lines
Typical OV HV BPL urban topology class	OV HV 1	Urban case A (main subclass)	3	$L_1=1,150\text{m}$, $L_2=12,125\text{m}$, $L_3=8,425\text{m}$, $L_4=3,300\text{m}$	$L_{b1}=27,600\text{m}$, $L_{b2}=17,200\text{m}$, $L_{b3}=33,100\text{m}$
Aggravated OV HV BPL urban topology class	OV HV 2	Urban case B (main subclass)	4	$L_1=125\text{m}$, $L_2=3,950\text{m}$, $L_3=3,275\text{m}$, $L_4=13,875\text{m}$, $L_5=3,775\text{m}$	$L_{b1}=19,000\text{m}$, $L_{b2}=22,700\text{m}$, $L_{b3}=17,100\text{m}$, $L_{b4}=18,000\text{m}$
OV HV BPL suburban topology class	OV HV 3	Suburban case (main subclass)	2	$L_1=9,025\text{m}$, $L_2=12,750\text{m}$, $L_3=3,225\text{m}$	$L_{b1}=46,800\text{m}$, $L_{b2}=13,400\text{m}$
OV HV BPL rural topology class	OV HV 4	Rural case (main subclass)	1	$L_1=3,750\text{m}$, $L_2=21,250\text{m}$	$L_{b1}=21,100\text{m}$
OV HV BPL “LOS” topology class	OV HV 5	“LOS” case (main subclass)	0	$L_1=25,000\text{m}$	-

3. Numerical Results and Discussion

In this Section, numerical results concerning the statistical channel attenuation modeling of transmission BPL networks are first presented. First, CASD parameters of iSHM and mSHM are computed for the indicative OV HV BPL topologies of the main subclasses of Table 1. Second, the maximum, average and minimum of OV HV BPL topology main subclass capacities for the CASDs of iSHM and mSHM are presented while the percentage change and the average absolute percentage change for the indicative OV HV BPL topologies of the main subclasses of Table 1 are reported. Third, since CASD parameters of iSHM and mSHM are well defined, the definition procedure of iSHM and mSHM is presented by focusing on the class mapping through two scenarios, namely: (i) iSHM definition procedure for OV HV BPL topologies; and (ii) mSHM definition procedure for OV HV BPL topologies. Fourth, observations regarding the simulation time of the aforementioned two scenarios are given. Note that the operation settings that are required for the fine operation of the statistical modeling in OV HV BPL networks are the same with the ones of OV MV BPL topologies that are reported in Secs.2.1-2.4 of [2] for the deterministic hybrid model, iSHM, mSHM and definition procedure, respectively.

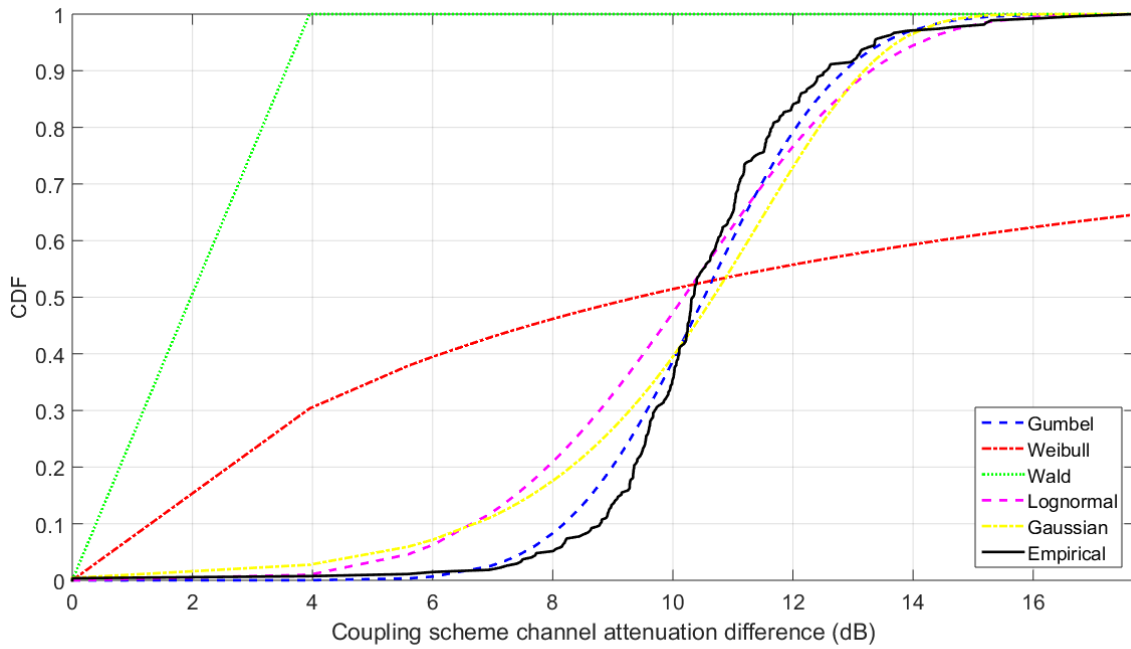
3.1 CASD MLEs of iSHM and mSHM of OV HV BPL Classes for the Default Operation Settings

The Business Process Modeling Notation (BPMN) diagrams of iSHM and mSHM, that describe the operation flowcharts of iSHM and mSHM, are given in Figs. 1(a) and 1(b) of [30], respectively. By comparing these flowcharts, the main difference between iSHM and mSHM is concentrated on the definition of the respective CASD parameters. As already been presented, the CASD parameters of iSHM are the CASD MLEs of Table 2 while the CASD parameter of mSHM is the Empirical CDF for given indicative BPL topology.

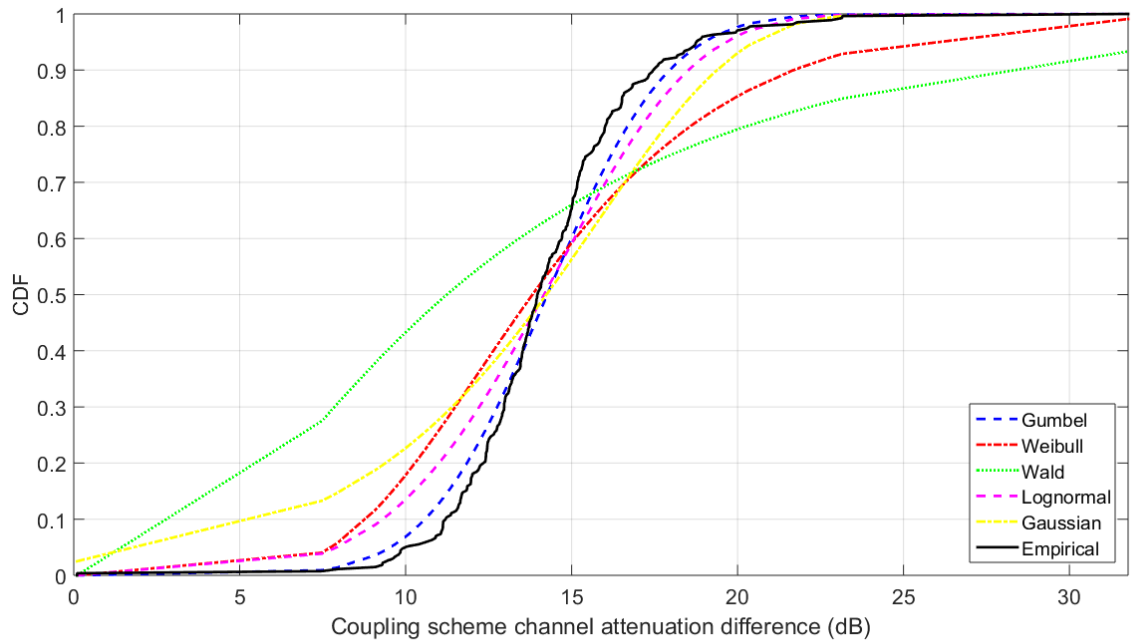
As the default operation settings are assumed, in Table 2, MLEs of the Gaussian, Lognormal, Wald, Weibull and Gumbel CASDs of iSHM are reported for the indicative OV HV BPL topologies of main subclasses of Table 1. With reference to Table 2, in Fig. 3(a), CDFs of the five channel attenuation statistical distributions (say, Gaussian, Lognormal, Wald, Weibull and Gumbel distributions) of the iSHM and of the Empirical CASD of the mSHM are plotted versus the coupling scheme channel attenuation difference for the case of the OV HV BPL urban case A. In Figs. 3(b)-(d), same plots with Fig. 3(a) are given but for the case of the OV HV BPL urban case B, suburban case and rural case, respectively.

Table 2
iSHM CASD MLEs of Indicative OV HV BPL Topologies for the Default Operation Settings

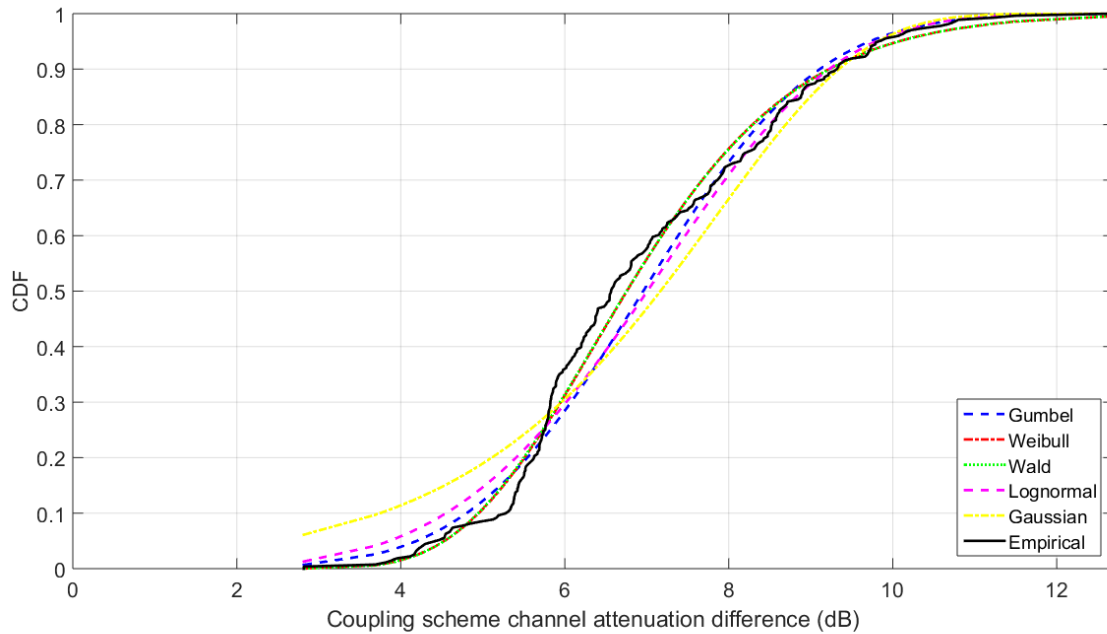
Topology Name	BPL Topology Class Description	iSHM									
		Gaussian MLEs		Lognormal MLEs		Wald MLEs		Weibull MLEs		Gumbel MLEs	
		$\hat{\mu}_{MLE}^{Gaussian}$	$\hat{\sigma}_{MLE}^{Gaussian}$	$\hat{\mu}_{MLE}^{Lognormal}$	$\hat{\sigma}_{MLE}^{Lognormal}$	$\hat{\mu}_{MLE}^{Wald}$	$\hat{\lambda}_{MLE}^{Wald}$	$\hat{\alpha}_{MLE}^{Weibull}$	$\hat{\beta}_{MLE}^{Weibull}$	$\hat{\alpha}_{MLE}^{Gumbel}$	$\hat{\epsilon}_{MLE}^{Gumbel}$
Urban case A	Typical OV HV BPL urban topology class	10.52	1.82	2.24	1.69	10.52	0	11.04	4.49	11.44	2.09
Urban case B	Aggravated OV HV BPL urban topology class	14.27	2.88	2.63	0.35	14.27	0.026×10^3	15.38	4.48	15.81	4.28
Suburban case	OV HV BPL suburban topology class	6.96	1.68	1.91	0.24	6.96	0.11×10^3	7.62	4.37	7.83	1.81
Rural case	OV HV BPL rural topology class	3.56	1.16	1.13	1.63	3.56	0	3.88	2.60	4.25	2.19
“LOS” case	OV HV BPL “LOS” transmission class	1×10^{-11}	0	-25.33	0	0	2.62×10^3	0	∞	0	0



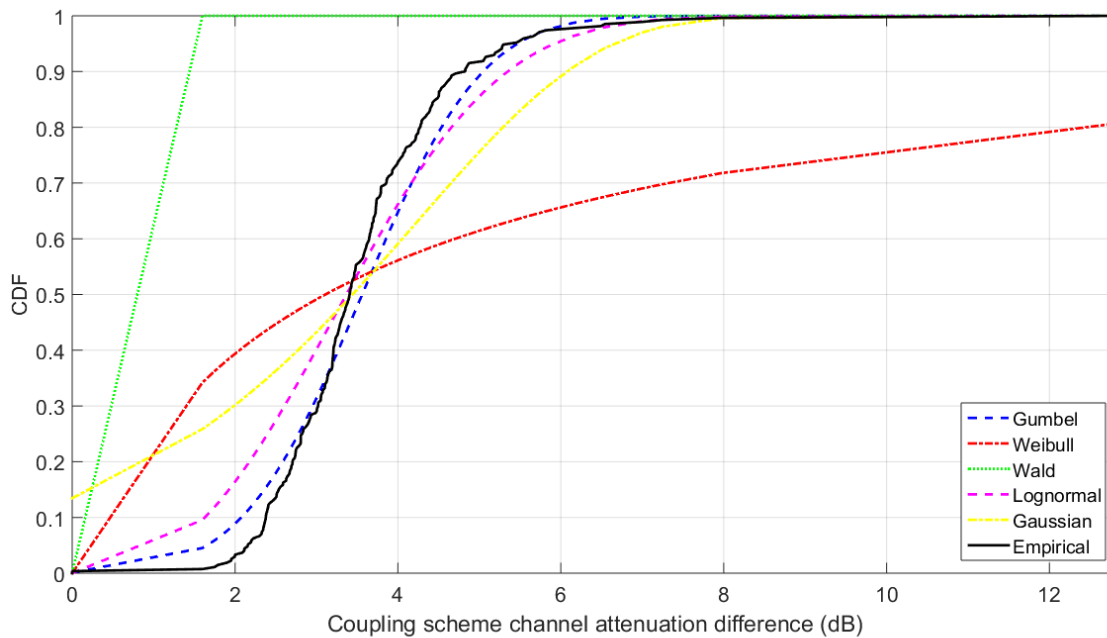
(a)



(b)



(c)



(d)

Fig. 3. CDFs of the indicative OV HV BPL topologies of Table 1 versus coupling scheme channel attenuation difference in the 3-30MHz frequency band when WtG¹ coupling scheme is deployed for CASDs of iSHM and mSHM. (a) Urban case A. (b) Urban case B. (c) Suburban case. (d) Rural case.

By comparing Table 2 with Table 1 of [29] and by observing Figs. 3(a)-(d), several comparative observations concerning CASD MLEs of iSHM and the CDF behavior of the CASDs of iSHM and mSHM can be presented, namely:

- Similarly to distribution BPL networks, as the complexity of the OV HV BPL topologies increase so do $\hat{\mu}_{MLE}^{Gaussian}$, $\hat{\mu}_{MLE}^{Lognormal}$, $\hat{\mu}_{MLE}^{Wald}$, $\hat{\alpha}_{MLE}^{Weibull}$ and $\hat{\alpha}_{MLE}^{Gumbel}$. Conversely to distribution BPL topologies, $\hat{\sigma}_{MLE}^{Gaussian}$, $\hat{\sigma}_{MLE}^{Lognormal}$, $\hat{\beta}_{MLE}^{Weibull}$ and $\hat{\epsilon}_{MLE}^{Gumbel}$ of OV HV BPL topologies receive significantly lower values than the respective ones of OV MV BPL topologies thus indicating that the variance of coupling scheme channel attenuation differences of OV HV BPL topologies remain lower than the respective ones of OV MV BPL topologies.
- $\hat{\mu}_{MLE}^{Gaussian}$, $\hat{\mu}_{MLE}^{Lognormal}$, $\hat{\mu}_{MLE}^{Wald}$, $\hat{\alpha}_{MLE}^{Weibull}$ and $\hat{\alpha}_{MLE}^{Gumbel}$ of OV HV BPL topologies receive values that are comparable to the respective ones of OV MV BPL topologies. This event indicates that the capacities of the main subclasses of OV HV BPL networks are expected to have: (i) comparable values to the capacities of the main subclasses of OV MV BPL networks; and (ii) comparable iSHM class maps to ones of OV MV BPL networks. Anyway, the capacities of the main subclasses determine the ones of the respective BPL topology classes.
- In contrast with Figs. 3(a), 3(b) and 3(d), CASD CDFs of Fig. 3(b) start to increase from a value different than zero. Actually, coupling scheme channel attenuation differences of OV HV BPL urban case A, urban case B and rural case present rare deep spectral notches that reach down to zero and, thus, their CASD CDFs start from zero. Anyway, this type of spectral notches is not present in OV HV BPL suburban case and for that reason its CASD CDFs start from approximately 3dB coupling scheme channel attenuation difference. Note that the coupling scheme channel attenuation differences of OV HV BPL topologies are restricted to range above zero since OV HV “LOS” case is characterized by the minimum coupling scheme channel attenuation due to the lack of branches across the transmission path.
- When the CASD CDF starts to increase at zero coupling scheme channel attenuation difference, certain CASD CDFs fail to follow the Empirical CASD CDF. In the cases of Figs. 3(a), 3(b) and 3(d), Wald and Weibull CASD CDFs present significant differences from the Empirical CDF since Wald CASD CDF expects to early handle the majority of data while Weibull CASD CDF expects to later handle the majority of data with respect to the aforementioned figures. Due to the previous observation, Wald CASD CDF early reaches up to 1 but Weibull CASD CDF later reaches up to 1. It is expected that these CDF deviations will also entail capacity deviations in OV HV BPL topologies and subclasses. In Fig. 3(c), CASD CDFs present similar behavior as the lack of zero coupling scheme channel attenuation difference forces CASD CDFs to almost coincide.
- By comparing Figs. 3(a)-(d) with respective Figs. 4(a)-(d) of [30], there are no coupling scheme channel attenuation difference horizontal steps in Empirical CDFs during the study of OV HV BPL topologies. In contrast with OV MV BPL topologies, there is no pattern regarding the depth, the extent and the location of spectral notches of OV HV BPL topologies and this has as a result a variety of values regarding the coupling scheme channel attenuation differences that further implies smooth Empirical CDFs with no horizontal steps.

In accordance with [2], [29], [30], it has been proven that the capacity performance success does not solely depend on the realism of random coupling scheme channel attenuation differences of the distribution BPL topology members, which are produced by the random number generator module of Phase D of iSHM and mSHM –see Figs. (2) and 2(b) of [1]–. In the following subsections, the capacity estimation performance, which is assessed by applying the metrics of capacity, capacity percentage change and average absolute capacity percentage change, is going to be investigated for the different CASDs of iSHM and mSHM.

3.2 CASD Capacities and Capacity Estimation Performance Metrics of OV HV BPL Main Subclasses for the Default Operation Settings

As the default operation settings are assumed, CASD parameters of iSHM and mSHM are reported in Table 2 and in Figs. 3(a)-(d), respectively. With respect to Table 1 and 2, each OV HV BPL topology main subclass is enriched with 100 topology members per each CASD through the random number generator of Phase D as described in [28]. Similarly to [29], [30], each OV HV BPL topology subclass can be described by the maximum, average and minimum capacity of its topology members while the corresponding capacity estimation performance metrics, say, capacity percentage change and average absolute capacity percentage change, can be computed. In accordance with [2], [29], although the graphical analysis can be very descriptive regarding the capacity estimation performance of CASDs of iSHM and mSHM, the capacity estimation performance of CASDs can also be examined by simply applying capacity estimation performance metrics of percentage change and average absolute percentage change. Therefore, the percentage change and the average absolute percentage change of each CASD of iSHM and mSHM are given in Table 3 per each indicative OV HV BPL topology main subclasses. Also, the capacity of the indicative OV HV BPL topologies of main subclasses of Table 1 is also reported in the first column of the Table.

Table 3

Percentage Change between the Average Capacity of the OV HV BPL Topology Class and the Capacity of the Indicative Topology of the Respective Class for the Five Examined CASDs of iSHM and the Empirical CASD of mSHM when the Default Operation Settings are assumed (say, WtG¹/StP¹ coupling scheme and FCC Part 15)

(grey background: best results, black background: unsuccessful capacity estimation)

Indicative OV HV BPL Topology Name (OV HV Capacity in Mbps)	BPL Topology Class Description	Percentage Change (%)					
		iSHM					mSHM
		Gaussian	Lognormal	Wald	Weibull	Gumbel	Empirical
Urban case A (187)	Typical BPL urban class	-0.0088	-15.44	50.57	2.13	1.38	0.15
Urban case B (153)	Aggravated BPL urban	0.0031	-1.73	5.52	1.46	5.01	0.38
Suburban case (218)	BPL suburban class	0.0025	-0.015	-0.0056	0.067	0.64	0.074

Rural case (249)	BPL rural class	-0.0045	-13.41	12.86	0.42	0.98	0.078
Average Absolute Percentage Change (%)		0.012	7.65	17.24	1.02	2.00	0.17

By comparing Table 3 with Table 3 of [29] and Table 3 of [30], significant similarities and differences that can be also explained by the study of Figs. 1(a)-(d) of [29] and Figs. 6(a)-(d) of [30] can be pointed out for the behavior of CASD capacity performance in OV HV BPL networks, namely:

- CASD capacity estimation performance for OV HV BPL subclasses presents significant similarities with the one of OV MV BPL topologies but also several differences. Although the typical transmission path of OV HV BPL topologies is typically equal to 25km and is significantly greater than the 1km typical transmission path of OV MV BPL topologies, the capacities of the indicative OV HV BPL topologies are slightly smaller than the respective capacities of the indicative OV MV BPL topologies. Actually, OV HV BPL topologies are characterized by a stronger “LOS” attenuation mechanism than the one of OV MV BPL topologies while the multipath aggravation in OV HV BPL topologies remains approximately the same with the one of OV MV BPL topologies [10].
- As already been mentioned in [29] for the distribution BPL subclasses, from the graphical perspective, a successful CASD capacity estimation performance should satisfy the following criteria: (i) capacity range of each transmission BPL topology subclass comprises the capacity of its respective indicative transmission BPL topology; and (ii) the average capacity value of the examined transmission BPL topology subclass remains very close to the respective one of the indicative transmission BPL topology. Without significant differences, the average capacity of each OV HV BPL topology subclass can be assumed to be equal to the capacity of its representative OV HV BPL topology. From the capacity estimation metric perspective, the lower the percentage change and average absolute percentage change in absolute values remain the better the capacity estimation performance is.
- Similarly to OV MV BPL topology subclasses, Weibull and Empirical CASDs succeed in satisfying either the aforementioned criteria for a successful capacity graphical estimation or the 3% threshold of percentage change and average absolute percentage change in all the OV HV BPL topology subclasses examined. But, apart from Weibull and Empirical CASDs, Gaussian CASD also succeeds in successfully estimating capacity of OV HV BPL subclasses with excellent performance. As the other CASDs are concerned, Lognormal, Wald and Gumbel fail in two, three and one OV HV BPL topology subclasses, respectively. More analytically, Lognormal CASD presents a mixed capacity estimation behavior since it successfully estimates the capacity of OV HV BPL urban case B and suburban case subclasses. In accordance with [29], [30], Wald CASD is more suitable for estimating capacities of BPL subclasses that are characterized by intense “LOS” attenuation and, for that reason, Wald CASD presents the best

results when UN MV BPL topology subclasses are examined. In OV HV BPL subclasses, Wald CASD only succeeds in estimating the capacity of OV HV BPL suburban case subclass. Conversely, Gumbel CASD can be considered as a general purpose CASD which prefers OV HV BPL subclasses of low multipath aggravation.

- By recognizing the similarities and the differences of CASD performance, it is evident that OV HV BPL topologies can be treated as a middle condition between OV MV and UN MV BPL topologies. More specifically, since OV HV BPL topologies suffer from both high “LOS” attenuation due to the high 25km “LOS” transmission path and intense multipath aggravation, Gaussian CASD behaves as the suitable CASD for these complicated communications environments. In fact, Gaussian CASD is the middle solution between the Weibull and Wald CASDs of OV MV and UN MV BPL topologies, respectively. With reference to Table 3, the average absolute percentage change of Gaussian, Weibull and Wald CASD is equal to 0.012% (best), 1.02% (successful capacity estimation) and 17.24% (unsuccessful capacity estimation), respectively. Here, it should be noted that Empirical CASD of mSHM

3.3 iSHM and mSHM Class Mapping for OV HV BPL Classes for the Default Operation Settings

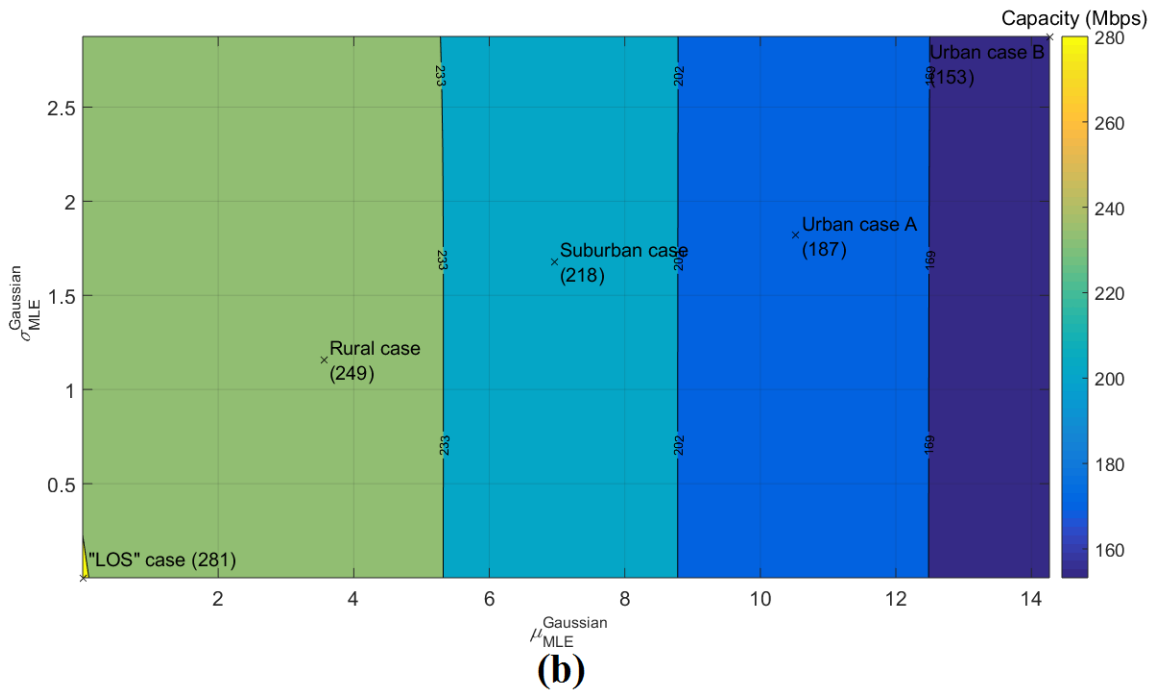
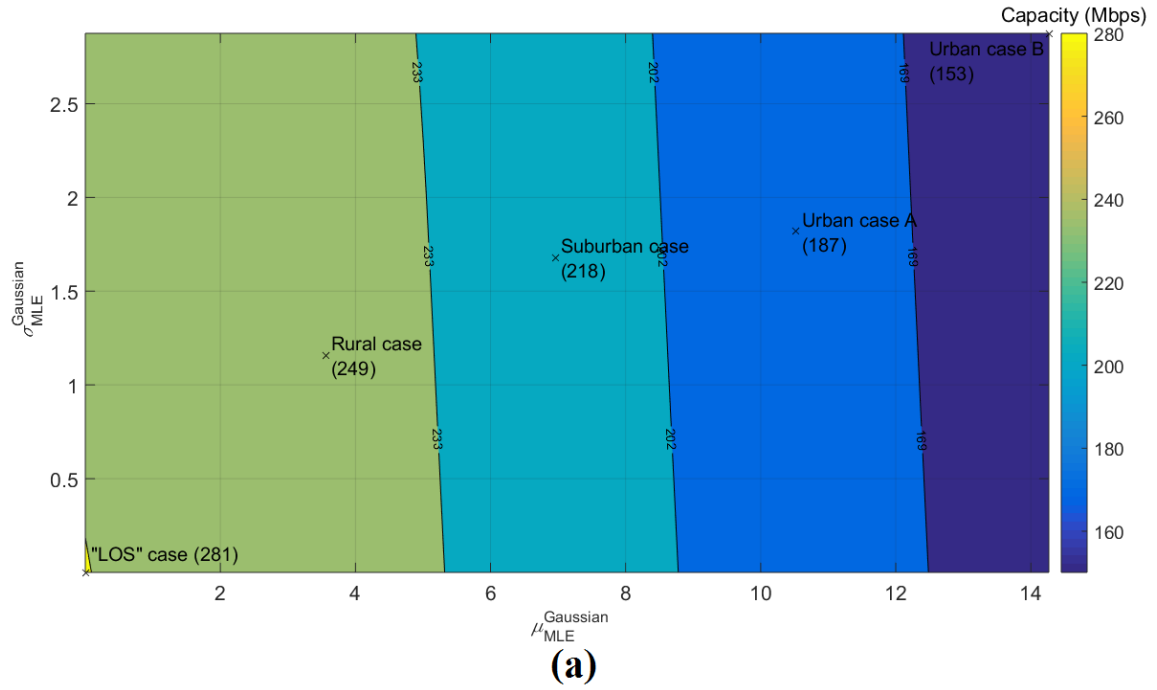
The definition procedures of iSHM and mSHM have been presented in [1] for the distribution BPL classes. For the case of OV HV BPL classes, two scenarios regarding the class mapping are here presented, namely: (i) iSHM definition procedure for OV HV BPL topologies; and (ii) mSHM definition procedure for OV HV BPL topologies.

As already been mentioned in Sec.3.2, Gaussian and Empirical CASDs are considered to execute successful capacity estimations because the average capacity values of the examined transmission BPL topology subclasses remain very close to the capacities of the respective indicative transmission BPL topologies. Apart from the average capacity value of the examined transmission BPL topology subclass, the minimum and maximum capacities of each transmission BPL topology subclass surround the capacity of its respective indicative transmission BPL topology while all three capacity values lie very close among them for the CASDs that execute successful capacity estimations in accordance with Figs. 1(a)-(d) of [29] and Figs. 6(a)-(d) of [30]. In this paper, the shift impact on the OV HV BPL topology class borderlines of iSHM and mSHM class maps is going to be examined when the minimum and the maximum capacities of each transmission BPL topology subclass are assumed to be applied instead of the average capacity of each subclass. The latter argument implies that the steps FL1.08 and FL2.08 of Figs. 3(a) and 3(b) of [1] that deal with the definition procedure of iSHM and mSHM, respectively, are going to be modified; instead of the computation of the average capacity of each virtual transmission BPL topology subclass, the minimum and maximum capacities are going to be considered.

As the iSHM class map scenario is concerned, with reference to Table 3, Gaussian CASD presents the best capacity estimation metric results among the other CASDs in OV HV BPL topologies. For the five indicative OV HV BPL topologies of the

main subclasses of Table 1, the respective $\hat{\mu}_{MLE}^{Gaussian}$ and $\hat{\sigma}_{MLE}^{Gaussian}$, which are the Gaussian CASD MLEs, are reported in Table 2 while the respective capacities are given in the first column of Table 3. Based on the Gaussian CASD MLEs and capacities of the five indicative OV HV BPL topologies of the main subclasses, the spacings for the horizontal and vertical axis are equal to $\frac{14.27-1 \times 10^{-11}}{10} = 1.427$ and $\frac{2.88-0}{10} = 0.288$, respectively, while the capacity borders between the adjacent distribution BPL topology classes $CB\sigma_l^{G,C}, l = 1, 2, 3, 4$ are equal to 169Mbps, 202Mbps, 233Mbps and 281Mbps, respectively.

The iSHM class map of OV HV BPL topologies is plotted in Fig. 4(a) with respect to $\hat{\mu}_{MLE}^{Gaussian}$ and $\hat{\sigma}_{MLE}^{Gaussian}$ for the default operation settings when the minimum capacity of each OV HV BPL topology subclass of step FL1.08 of Fig.3(a) of [1] is considered instead of the average capacity. In the same class map, the Gaussian CASD MLEs of the five indicative OV HV BPL topologies of the main subclasses of Table 1 with the corresponding capacities are also shown. In Figs. 4(b) and 4(c), same plots with Fig. 4(a) are demonstrated but for the case of average and maximum capacities, respectively.



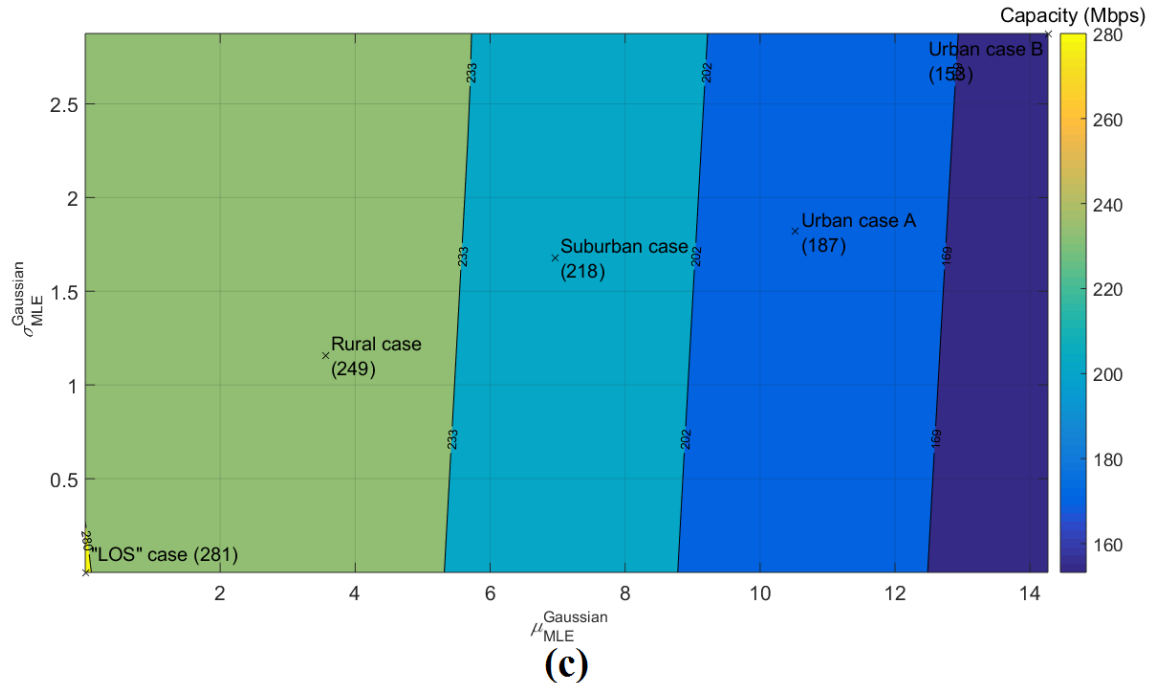
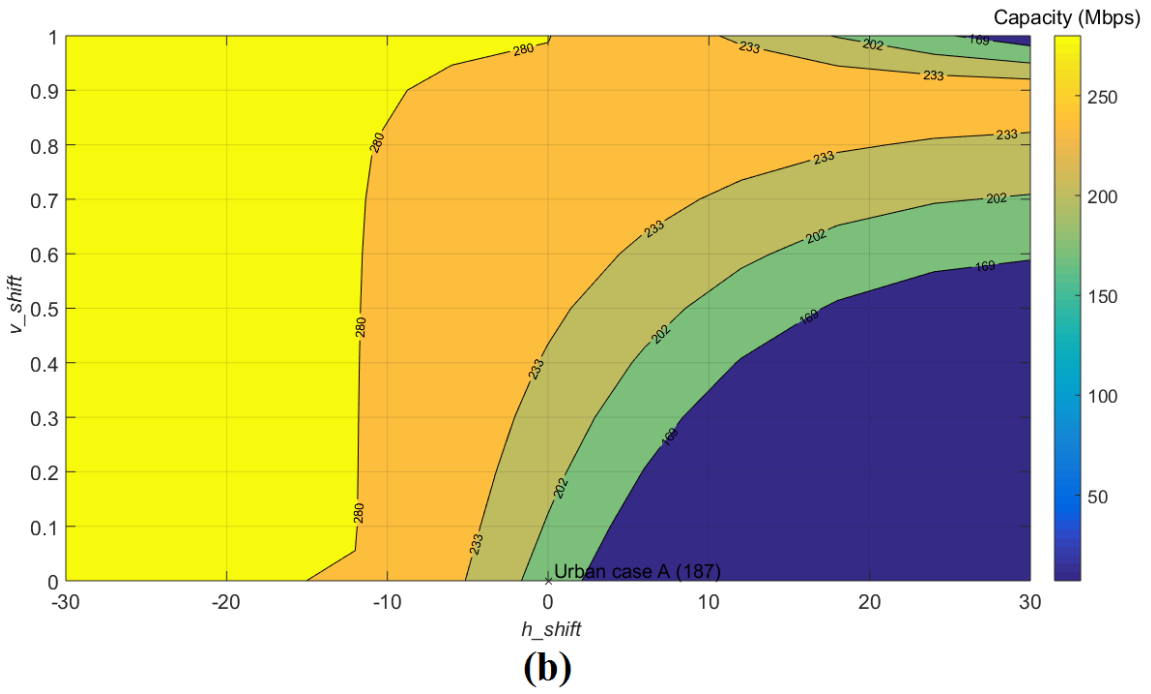
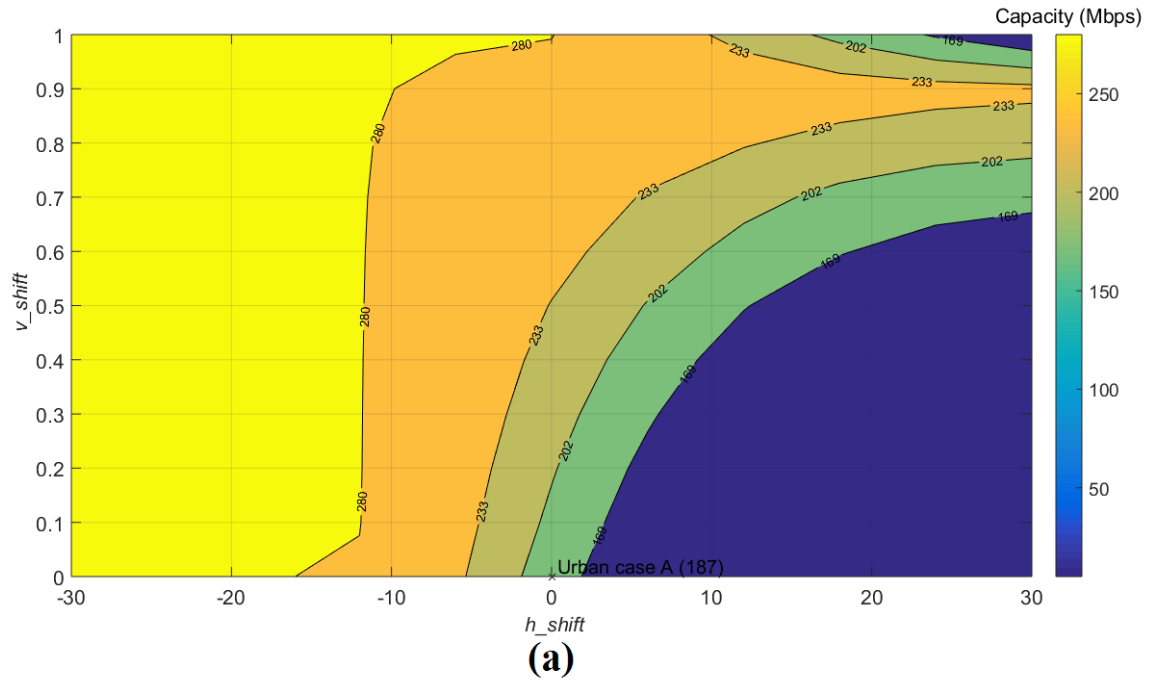


Fig. 4. iSHM class map of the OV HV BPL topologies in the 3-30MHz frequency band when WtG¹ coupling scheme is deployed and FCC Part 15 is applied. (a) Minimum capacities of OV HV BPL topology subclasses. (b) Average capacities of OV HV BPL topology subclasses. (c) Maximum capacities of OV HV BPL topology subclasses.

As the mSHM class map scenario is concerned, in accordance with [1], [2], all the four indicative OV HV BPL topologies of the main subclasses of Table 1, except for the OV HV “LOS” case, are examined separately during the preparation of mSHM class maps. Since the behavior of different indicative OV HV BPL topologies of the main subclasses has been examined in [2], only one of the indicative OV HV BPL topologies of the main subclasses is going to be examined in this paper, say, the OV HV BPL urban case A. As the horizontal shifts, vertical shifts, horizontal shift spacings and vertical shift spacings of the mSHM class maps of OV HV BPL topologies are considered, these are assumed to receive the same values with the respective ones of the mSHM class maps of OV MV and UN MV BPL topologies, which are reported in [2]; say, the maximum and minimum horizontal shift is assumed to be equal to 30dB and -30dB, respectively, while the maximum and minimum vertical shift is assumed to be equal to 1 and 0, respectively. The capacity borders between the adjacent OV HV BPL topology classes $CB\sigma_l^{G,C}, l = 1, 2, 3, 4$ are equal to the respective capacity borders during the preparation of the iSHM class maps.

The mSHM class map of OV HV BPL topologies is plotted in Fig. 5(a) with respect to the horizontal shift h_shift and vertical shift v_shift for the default operation settings when the minimum capacity of each OV HV BPL topology subclass of step FL2.08 of Fig.3(b) of [1] is assumed. In the same 2D contour plot, the capacity borders between the adjacent transmission BPL topology classes and the capacity of the reference indicative OV HV BPL urban case A of Table 1 are also shown. In Figs. 5(b) and 5(c), same plots with Fig. 5(a) are demonstrated but for the case of average and maximum capacities, respectively.



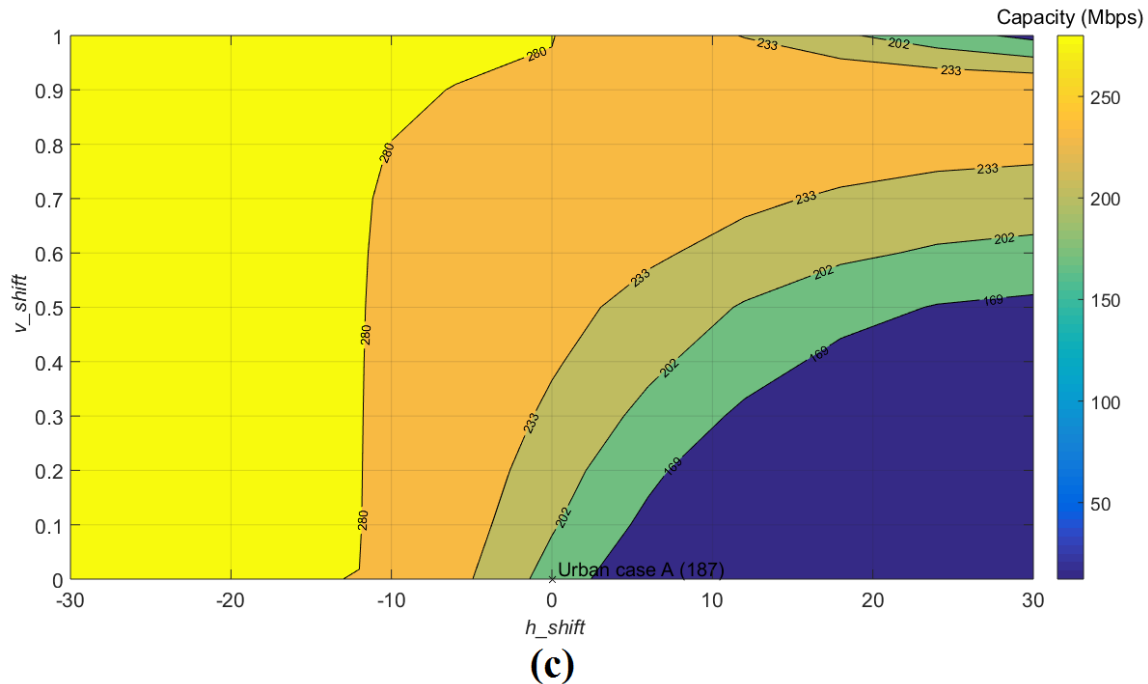


Fig. 5. mSHM class map of the OV HV BPL topologies in the 3-30MHz frequency band when StP¹ coupling scheme is deployed and FCC Part 15 is applied for reference indicative OV HV BPL urban case A. (a) Minimum capacities of OV HV BPL topology subclasses. (b) Average capacities of OV HV BPL topology subclasses. (c) Maximum capacities of OV HV BPL topology subclasses.

By observing Figs. 4(a)-(c) and Figs. 5(a)-(c), several interesting conclusions can be reported concerning the iSHM and mSHM class maps, namely:

- By comparing iSHM class maps of OV HV BPL topologies against iSHM class maps of OV MV and UN MV BPL topologies, which are presented in [2], iSHM class maps of OV HV BPL topologies present more similarities to the iSHM class maps of UN MV BPL topologies due to the existence of five almost rectangle capacity areas between the computed borders; say, the slope of the capacity area borderlines relative to the horizontal axis is almost equal to 90 degrees. As the mSHM class maps of OV HV BPL topologies are concerned, these are similar in format to the mSHM class maps of OV MV and UN MV BPL topologies, which are presented in [2]. Anyway, the mSHM class maps are characterized by a large left capacity area of respective “LOS” case capacity value while a large capacity degrading area at the bottom right side of the class maps occurs.
- Similarly to $\hat{\alpha}_{MLE}^{Weibull}$ and $\hat{\mu}_{MLE}^{Wald}$ of OV MV and UN MV BPL topology subclasses, respectively, in iSHM class maps of [2], as the multipath environment of the examined OV HV BPL topologies becomes more intense with frequent and deep spectral notches, this has as a result the value increase of $\hat{\mu}_{MLE}^{Gaussian}$ and $\hat{\sigma}_{MLE}^{Gaussian}$. Hence, OV HV BPL urban topologies tend to be located at the right areas of the class map while the OV HV BPL rural topologies tend to be located at the left areas.

- By comparing Figs. 4(a)-(c) of iSHM class maps, there are differences concerning the slope of the capacity area borderlines when the minimum, the average and the maximum capacity of each transmission BPL topology subclass are considered, respectively. Actually, when the minimum capacity of the OV HV BPL topology subclasses is assumed, the slope of the capacity area borderlines relative to the horizontal axis becomes more than 90 degrees whereas the slope of the capacity area borderlines relative to the horizontal axis becomes less than 90 degrees when the maximum capacity of the OV HV BPL topology subclasses is considered. This is due to the fact that $\sigma_{MLE}^{Gaussian}$ of eq. (A3) of [28] can be treated as the variance of the normal distribution that describes the deviation of a random coupling scheme channel attenuation difference from its mean while $\mu_{MLE}^{Gaussian}$ of eq.(A2) of [28] describes the mean. Hence, as $\sigma_{MLE}^{Gaussian}$ increases for given $\mu_{MLE}^{Gaussian}$, so decreases the minimum capacity of the OV HV BPL topology subclasses that anyway depends on the coupling scheme channel attenuation thus having as effect the shift of the capacity areas to the left. The opposite effect holds for the study of the maximum capacity of the OV HV BPL topology subclass, where the increase of $\sigma_{MLE}^{Gaussian}$ triggers the increase of the maximum capacity of the OV HV BPL topology subclasses.
- Similarly to the iSHM class map of Fig. 4(b), mSHM class maps of Fig. 5(b) can support a plethora of virtual OV HV BPL topology subclasses by simply identifying the five capacity areas and by setting the corresponding pair of horizontal and vertical shifts of the coupling scheme channel attenuation of the reference OV HV BPL topology; say OV HV BPL urban case A.
- By comparing Figs. 5(a)-(c), it is obvious that the selection among the minimum, average and maximum capacity of each OV HV BPL topology subclass has very small impact on the location of capacity area borderlines of mSHM class maps (*i.e.*, the shift of the capacity area borderlines is almost zero) and this is due to the definition procedure of mSHM, which has been presented in [1]. By comparing steps FL1.06 of iSHM of Fig.3(a) of [1] and FL2.06 of mSHM of Fig.3(b) of [1], the modification of CASD MLEs of iSHM and the creation of CASD MLE pairs have as a result the definition of new virtual CDFs that are characterized by different CDF characteristics than the indicative CDF ones. Conversely, the definition of horizontal and vertical shifts of mSHM and the creation of Empirical CDF shift pair have as a result the definition of new virtual CDFs that are related in format to the representative Empirical CDF. Note that the successful capacity estimation performance of Empirical CASD implies that the average capacity value of all the examined OV HV BPL topology subclasses remain close to the respective minimum and maximum capacity values, as already been mentioned in Sec.3.2, and the latter observation combined with the simple linear modifications of the representative Empirical CDF through the horizontal and vertical shifts is reflected on the capacity range of all the examined OV HV BPL topology subclasses and, thus, on the small impact on the location of capacity area borderlines of mSHM class maps.

With reference to Table 3, although the capacity performance metrics of Gaussian CASD of iSHM and Empirical CASD of mSHM reveal the capacity estimation success of the aforementioned CASDs, the metrics of Gaussian CASD are better than the ones of

Empirical CASD. However, a possible trade-off between the capacity estimation performance and the simulation time, which has been proposed in [2], should be examined in this paper for the OV HV BPL topologies; say, the simulation time of Gaussian CASD capacity estimation performance is examined against the respective one of Empirical CASD in Sec.3.4.

3.4 iSHM and mSHM Class Map Simulation Times for OV HV BPL Classes for the Default Operation Settings

The trade-off between the capacity performance metrics and the simulation time of class mapping, which has been proposed in [2], for given CASD is investigated for OV HV BPL classes in this Section. Already been identified in Table 3, different CASDs achieve various capacity estimation performances with respect to the percentage change and the average absolute percentage change. Despite the capacity estimation performance, a reliable CASD should, at the same time, be a successful one and also be characterized by short simulation times of class mapping so that it can provide fast and reliable results thus having practical interest. In [30], it has been shown that Wald CASD of iSHM performs the best capacity estimation performance among all CASDs of iSHM and mSHM but Empirical CASD of mSHM that also performs an excellent capacity estimation performance has almost 30 times shorter simulation time than the Wald CASD. As the OV HV BPL topologies are concerned, in Fig. 6, the simulation time of class mapping is plotted against the number of spacings for the Gaussian CASD of iSHM and Empirical CASD of mSHM when OV HV BPL urban case A is assumed.

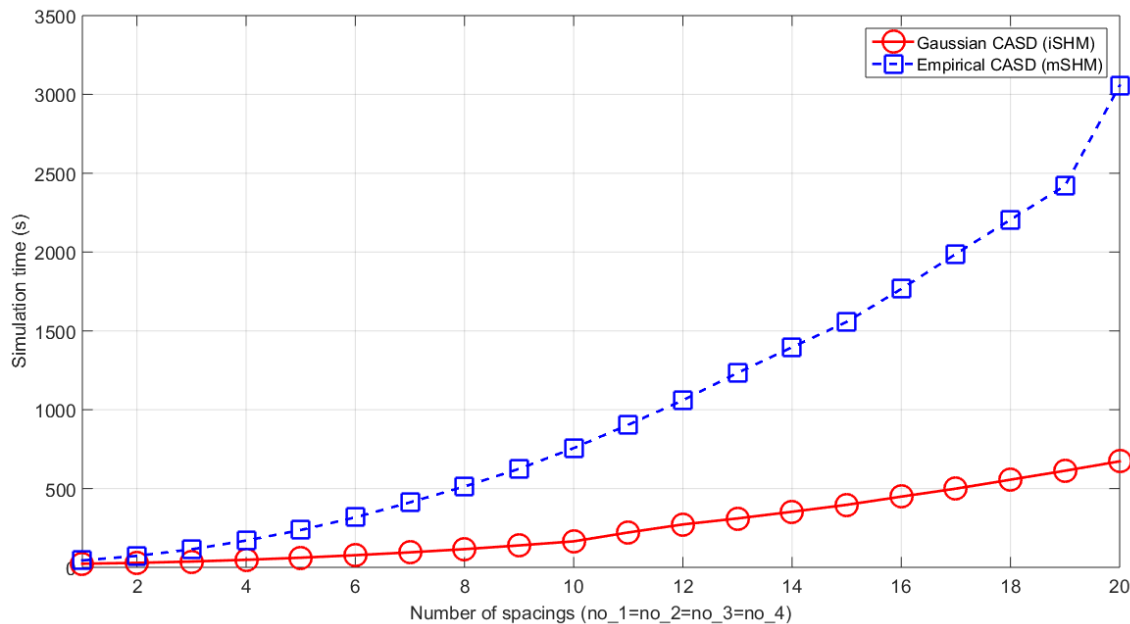


Fig. 6. Class map simulation time of the OV HV BPL urban case A in the 3-30MHz frequency band for WtG¹ coupling scheme and FCC Part 15 when different CASDs are applied and different number of spacings is used.

Note that the number of spacings (*i.e.*, no_1, no_2, no_3 and no_4) of the default operation settings is assumed to be equal to 10 either for the iSHM class maps or the mSHM class maps. From Fig. 6, the simulation time of the Gaussian CASD and Empirical CASD is equal to 164.9s and 756.3s, respectively, when the default operation settings are assumed. If the aforementioned simulation times are compared against the ones of Table 1 of [2] where the default operation settings have also been adopted, it is clear that the Empirical CASD simulation time of OV HV BPL class mapping is almost equal to the simulation time of the Empirical CASD OV MV and UN MV BPL class mapping since the larger part of the simulation time is consumed during the SHM phases and steps of the definition procedure rather than the deterministic hybrid model. As the Gaussian CASD is examined, its simulation time of OV HV BPL class mapping is significantly low and remains the lowest among the simulation times of Table 1 of [2] when the default operation settings are assumed. This indicates that the Gaussian CASD remains a reliable CASD for the preparation of the OV HV BPL class maps since it succeeds in providing the best capacity estimation results at the best simulation time.

But the main concern of the preparation of Fig. 6 is to explain the impact of the number of spacings on the simulation time of class mapping. Briefly presented in [2], the class mapping complexity is quadratic and this fact is verified in Fig. 6 either for Empirical CASD or the Gaussian CASD; *e.g.*, the expected simulation time for 20 segments is almost four times greater than the expected simulation time for 10 segments. Small differences are due to the simulation time required for the operation of the other SHM phases, steps of the definition procedure rather and the deterministic hybrid model. Regardless of the number of spacings, Gaussian CASD presents significantly lower simulation times in comparison with the one of the Empirical CASD. Hence, there is no trade-off relation between the simulation time and the capacity estimation performance in OV HV BPL topologies hence Gaussian CASD can be treated as the most reliable CASD among the examined CASDs in iSHM and mSHM for the OV HV BPL networks.

4. Conclusions

In this paper, the numerical results concerning the application of SHM (*i.e.*, both iSHM and mSHM) to OV HV BPL topologies have first been presented. Initially, the CASD parameters of iSHM and mSHM have been computed for the indicative OV HV BPL topologies of the main subclasses. Then, with respect to the percentage change and the average absolute percentage change, Gaussian CASD of iSHM and Empirical CASD of mSHM have been reported. Gaussian CASD can be considered as the middle solution between the Weibull CASD and Wald CASD that are anyway considered as the most successful iSHM CASD for the OV MV and UN MV BPL topologies, respectively, and this is due to the fact that the transmission characteristics of OV HV BPL topologies can be treated as the mix of transmission characteristics of OV MV and UN MV BPL topologies. Moreover, on the basis of the Gaussian CASD and the Empirical CASD, the definition procedure, which has already been reported for distribution BPL topologies, has first applied to transmission BPL

topologies. The iSHM and mSHM class maps of OV HV BPL topologies have first been presented while the differences between distribution and transmission BPL topologies have been highlighted. In this paper, the impact of considering the maximum, the average and the minimum values of BPL topology subclasses instead of only the average value has been highlighted and explained. Furthermore, the trade-off between the simulation time and the capacity estimation performance has been checked if it is valid in OV HV BPL topologies. Already been identified in UN MV BPL topologies, the aforementioned trade-off is not valid in OV HV BPL topologies where Gaussian CASD can be considered the most reliable CASD; say, Gaussian CASD achieves better capacity performance metrics and simulation time than the respective ones of Empirical CASD. Finally, the impact of the number of spacings on the simulation time has been demonstrated validating the quadratic time complexity, which has theoretically explained in [2]. After the application of SHM to transmission BPL networks, new virtual transmission BPL topologies and topology subclasses can be defined that can help towards various smart grid simulation scenarios that involve power line communications technology.

CONFLICTS OF INTEREST

The author declares that there is no conflict of interests regarding the publication of this paper.

References

- [1] A. G. Lazaropoulos, "Virtual Indicative Broadband over Power Lines Topologies for Respective Subclasses by Adjusting Channel Attenuation Statistical Distribution Parameters of Statistical Hybrid Models – Part 1: Theory," *Trends in Renewable Energy*, vol. 5, no. 3, pp 237-257, Aug. 2019. DOI: 10.17737/tre.2019.5.3.0099
- [2] A. G. Lazaropoulos, "Virtual Indicative Broadband over Power Lines Topologies for Respective Subclasses by Adjusting Channel Attenuation Statistical Distribution Parameters of Statistical Hybrid Models – Part 2: Numerical Results for the Overhead and Underground Medium-Voltage Power Grids," *Trends in Renewable Energy*, vol. 5, no. 3, pp 258-281, Aug. 2019. DOI: 10.17737/tre.2019.5.3.00100
- [3] A. G. Lazaropoulos, "Review and Progress towards the Capacity Boost of Overhead and Underground Medium-Voltage and Low-Voltage Broadband over Power Lines Networks: Cooperative Communications through Two- and Three-Hop Repeater Systems," *ISRN Electronics*, vol. 2013, Article ID 472190, pp. 1-19, 2013. [Online]. Available: <http://www.hindawi.com/isrn/electronics/aip/472190/>
- [4] A. G. Lazaropoulos, "Deployment Concepts for Overhead High Voltage Broadband over Power Lines Connections with Two-Hop Repeater System: Capacity Countermeasures against Aggravated Topologies and High Noise

- Environments,” *Progress in Electromagnetics Research B*, vol. 44, pp. 283-307, 2012. [Online]. Available: <http://www.jpier.org/PIERB/pierb44/13.12081104.pdf>
- [5] A. G. Lazaropoulos and P. G. Cottis, “Transmission characteristics of overhead medium voltage power line communication channels,” *IEEE Trans. Power Del.*, vol. 24, no. 3, pp. 1164-1173, Jul. 2009.
- [6] A. G. Lazaropoulos and P. G. Cottis, “Capacity of overhead medium voltage power line communication channels,” *IEEE Trans. Power Del.*, vol. 25, no. 2, pp. 723-733, Apr. 2010.
- [7] A. G. Lazaropoulos and P. G. Cottis, “Broadband transmission via underground medium-voltage power lines-Part I: transmission characteristics,” *IEEE Trans. Power Del.*, vol. 25, no. 4, pp. 2414-2424, Oct. 2010.
- [8] A. G. Lazaropoulos and P. G. Cottis, “Broadband transmission via underground medium-voltage power lines-Part II: capacity,” *IEEE Trans. Power Del.*, vol. 25, no. 4, pp. 2425-2434, Oct. 2010.
- [9] A. G. Lazaropoulos, “Broadband transmission and statistical performance properties of overhead high-voltage transmission networks,” *Hindawi Journal of Computer Networks and Commun.*, 2012, article ID 875632, 2012. [Online]. Available: <http://www.hindawi.com/journals/jcnc/aip/875632/>
- [10] A. G. Lazaropoulos, “Towards Modal Integration of Overhead and Underground Low-Voltage and Medium-Voltage Power Line Communication Channels in the Smart Grid Landscape: Model Expansion, Broadband Signal Transmission Characteristics, and Statistical Performance Metrics (Invited Paper),” *ISRN Signal Processing*, vol. 2012, Article ID 121628, pp. 1-17, 2012. [Online]. Available: <http://www.hindawi.com/isrn/sp/2012/121628/>
- [11] D. G. Della amd S. Rinaldi, “Hybrid Communication Network for the Smart Grid: Validation of a Field Test Experience,” *IEEE Trans. Power Del.*, vol. 30, no. 6, pp. 2492-2500, 2015.
- [12] F. Versolatto and A. M. Tonello, “An MTL theory approach for the simulation of MIMO power-line communication channels,” *IEEE Trans. Power Del.*, vol. 26, no. 3, pp. 1710-1717, Jul. 2011.
- [13] P. Amirshahi and M. Kavehrad, “High-frequency characteristics of overhead multiconductor power lines for broadband communications,” *IEEE J. Sel. Areas Commun.*, vol. 24, no. 7, pp. 1292-1303, Jul. 2006.
- [14] L. Stadelmeier, D. Schneider, D. Schill, A. Schwager, and J. Speidel, “MIMO for inhome power line communications,” presented at the *Int. Conf. on Source and Channel Coding*, Ulm, Germany, Jan. 2008.
- [15] T. Sartenaer, “Multiuser communications over frequency selective wired channels and applications to the powerline access network” *Ph.D. dissertation*, Univ. Catholique Louvain, Louvain-la-Neuve, Belgium, Sep. 2004.
- [16] T. Calliacoudas and F. Issa, ““Multiconductor transmission lines and cables solver,” An efficient simulation tool for plc channel networks development,” presented at the *IEEE Int. Conf. Power Line Communications and Its Applications*, Athens, Greece, Mar. 2002.
- [17] S. Galli and T. Banwell, “A deterministic frequency-domain model for the indoor power line transfer function,” *IEEE J. Sel. Areas Commun.*, vol. 24, no. 7, pp. 1304-1316, Jul. 2006.

- [18] S. Galli and T. Banwell, "A novel approach to accurate modeling of the indoor power line channel-Part II: Transfer function and channel properties," *IEEE Trans. Power Del.*, vol. 20, no. 3, pp. 1869-1878, Jul. 2005.
- [19] A. Pérez, A. M. Sánchez, J. R. Regué, M. Ribó, R. Aquilué, P. Rodríguez-Cepeda, and F. J. Pajares, "Circuitual and modal characterization of the power-line network in the PLC band," *IEEE Trans. Power Del.*, vol. 24, no. 3, pp. 1182-1189, Jul. 2009.
- [20] T. Sartenaer and P. Delogne, "Deterministic modelling of the (Shielded) outdoor powerline channel based on the multiconductor transmission line equations," *IEEE J. Sel. Areas Commun.*, vol. 24, no. 7, pp. 1277-1291, Jul. 2006.
- [21] T. Sartenaer and P. Delogne, "Powerline cables modelling for broadband communications," in Proc. *IEEE Int. Conf. Power Line Communications and Its Applications*, Malmö, Sweden, Apr. 2001, pp. 331-337.
- [22] C. R. Paul, *Analysis of Multiconductor Transmission Lines*. New York: Wiley, 1994.
- [23] J. A. B. Faria, *Multiconductor Transmission-Line Structures: Modal Analysis Techniques*. New York: Wiley, 1994.
- [24] H. Meng, S. Chen, Y. L. Guan, C. L. Law, P. L. So, E. Gunawan, and T. T. Lie, "Modeling of transfer characteristics for the broadband power line communication channel," *IEEE Trans. Power Del.*, vol. 19, no. 3, pp. 1057-1064, Jul. 2004.
- [25] A. Semlyen and B. Gustavsen, "Phase-domain transmission-line modeling with enforcement of symmetry via the propagated characteristic admittance matrix," *IEEE Trans. Power Del.*, vol. 27, no. 2, pp. 626-631, Apr. 2012.
- [26] A. M. Tonello and F. Versolatto, "Bottom-up statistical PLC channel modeling—Part I: Random topology model and efficient transfer function computation," *IEEE Transactions on Power Delivery*, vol. 26, no. 2, pp. 891-898, 2011.
- [27] A. M. Tonello and F. Versolatto, "Bottom-up statistical PLC channel modeling—Part II: Inferring the statistics," *IEEE transactions on Power Delivery*, vol. 25, no. 4, pp. 2356-2363, 2010.
- [28] A. G. Lazaropoulos, "Statistical Broadband over Power Lines Channel Modeling – Part 1: The Theory of the Statistical Hybrid Model," *Progress in Electromagnetics Research C*, vol. 92, pp. 1-16, 2019. [Online]. Available: <http://www.jpier.org/PIERC/pierc92/01.19012902.pdf>
- [29] A. G. Lazaropoulos, "Statistical Broadband over Power Lines (BPL) Channel Modeling – Part 2: The Numerical Results of the Statistical Hybrid Model," *Progress in Electromagnetics Research C*, vol. 92, pp. 17-30, 2019. [Online]. Available: <http://www.jpier.org/PIERC/pierc92/02.19012903.pdf>
- [30] A. G. Lazaropoulos, "Enhancing the Statistical Hybrid Model Performance in Overhead and Underground Medium Voltage Broadband over Power Lines Channels by Adopting Empirical Channel Attenuation Statistical Distribution," *Trends in Renewable Energy*, vol. 5, no. 2, pp. 181-217, 2019. [Online]. Available: <http://futureenergysp.com/index.php/tre/article/view/96/pdf>
- [31] T. Oliveira, A. Picorone, C. Zeller, S. Netto, and M. Ribeiro, "Statistical Modeling of Brazilian In-Home PLC Channel Features," *Journal of Communication and Information Systems*, vol. 34, no. 1, pp. 154-168, 2019.

- [32] T. R. Oliveira, C. B. Zeller, S. L. Netto, and M. V. Ribeiro, "Statistical modeling of the average channel gain and delay spread in in-home PLC channels," in *Proc. in IEEE International Symposium on Power Line Communications and Its Applications*, pp. 184-188, Mar. 2015.
- [33] J. A. Cortes, F. J. Canete, L. Diez, and J. L. G. Moreno, "On the statistical properties of indoor power line channels: Measurements and models," in *Proc. IEEE International Symposium on Power Line Communications and Its Applications*, pp. 271-276, Apr. 2011.
- [34] A. G. Lazaropoulos, "Towards Broadband over Power Lines Systems Integration: Transmission Characteristics of Underground Low-Voltage Distribution Power Lines," *Progress in Electromagnetics Research B*, vol. 39, pp. 89-114, 2012. [Online]. Available: <http://www.jpier.org/PIERB/pierb39/05.12012409.pdf>
- [35] A. Heathcote, S. Brown, and D. Cousineau, "QMPE: Estimating Lognormal, Wald, and Weibull RT distributions with a parameter-dependent lower bound," *Behavior Research Methods, Instruments, & Computers*, vol. 36, no. 2, pp. 277-290, 2004.
- [36] N. Suljanović, A. Mujčić, M. Zajc, and J. F. Tasič, "Approximate computation of high-frequency characteristics for power line with horizontal disposition and middle-phase to ground coupling," *Elsevier Electr. Power Syst. Res.*, vol. 69, pp. 17-24, Jan. 2004.
- [37] N. Suljanović, A. Mujčić, M. Zajc, and J. F. Tasič, "High-frequency characteristics of high-voltage power line," in *Proc. IEEE Int. Conf. on Computer as a Tool*, Ljubljana, Slovenia, Sep. 2003, pp. 310-314.
- [38] N. Suljanović, A. Mujčić, M. Zajc, and J. F. Tasič, "Power-line high-frequency characteristics: analytical formulation," in *Proc. Joint 1st Workshop on Mobile Future & Symposium on Trends in Communications*, Bratislava, Slovakia, Oct. 2003, pp. 106-109.
- [39] W. Villiers, J. H. Cloete, and R. Herman, "The feasibility of ampacity control on HV transmission lines using the PLC system," in *Proc. IEEE Conf. Africon*, George, South Africa, Oct. 2002, vol. 2, pp. 865-870.
- [40] P. Amirshahi, "Broadband access and home networking through powerline networks" Ph.D. dissertation, Pennsylvania State Univ., University Park, PA, May 2006.
- [41] M. D'Amore and M. S. Sarto, "A new formulation of lossy ground return parameters for transient analysis of multiconductor dissipative lines," *IEEE Trans. Power Del.*, vol. 12, no. 1, pp. 303-314, Jan. 1997.
- [42] P. Amirshahi and M. Kavehrad, "Medium voltage overhead powerline broadband communications; Transmission capacity and electromagnetic interference," in *Proc. IEEE Int. Symp. Power Line Commun. Appl.*, Vancouver, BC, Canada, Apr. 2005, pp. 2-6.
- [43] M. D'Amore and M. S. Sarto, "Simulation models of a dissipative transmission line above a lossy ground for a wide-frequency range-Part I: Single conductor configuration," *IEEE Trans. Electromagn. Compat.*, vol. 38, no. 2, pp. 127-138, May 1996.
- [44] M. D'Amore and M. S. Sarto, "Simulation models of a dissipative transmission line above a lossy ground for a wide-frequency range-Part II: Multi-conductor

- configuration,” *IEEE Trans. Electromagn. Compat.*, vol. 38, no. 2, pp. 139-149, May 1996.
- [45] A. G. Lazaropoulos, “A Panacea to Inherent BPL Technology Deficiencies by Deploying Broadband over Power Lines (BPL) Connections with Multi-Hop Repeater Systems,” *Bentham Recent Advances in Electrical & Electronic Engineering*, vol. 10, no. 1, pp. 30-46, 2017.

Article copyright: © 2019 Athanasios G. Lazaropoulos. This is an open access article distributed under the terms of the [Creative Commons Attribution 4.0 International License](https://creativecommons.org/licenses/by/4.0/), which permits unrestricted use and distribution provided the original author and source are credited.

